International Journal of Heat and Mass Transfer 52 (2009) 4635–4649

Contents lists available at ScienceDirect

International Journal of Heat and Mass Transfer

journal homepage: www.elsevier.com/locate/ijhmt

Effect of rib height on heat transfer in a two pass rectangular channel (*AR* = 1:4) with a sharp entrance at high rotation numbers

Michael Huh, Yao-Hsein Liu, Je-Chin Han *

Texas A&M University, Dept. of Mechanical Engineering, College Station, TX 77843, USA

ARTICLE INFO

Article history:
Received 21 July 2008
Received in revised form 3 March 2009
Available online 4 May 2009

Keywords:
Heat transfer
Rotating rectangular channel
Rotation number
Buoyancy parameter
Internal cooling

ABSTRACT

Blockage ratio effects on heat transfer in 1:4 *AR* channels with developing flow is experimentally determined. The blockage ratios (e/D_h) were 0.078 and 0.156. Reynolds numbers up to 40 K and rotational speeds up to 400 rpm were considered. The rotation number (*Ro*) and local buoyancy parameter (Bo_x) were extended to 0.65 and 1.5, respectively. The entrance dominates over rotation on the trailing surface first pass. The leading surface is dominated by rotation. Rotation effects are reduced by the ribs and heat transfer is similar for both walls in the second pass. Rotation effects were similar for both blockage ratios. The correlations show that the buoyancy parameter is useful to predict heat transfer in the extended range.

1. Introduction

Gas turbine blades are exposed to temperatures considerably above the melting point of the metals which are used in the manufacturing process. To protect the blades in such harsh environments, various blade cooling techniques are employed. For example, film cooling is used to help insulate the external blade surface with a layer of relatively cooler air that is injected through holes on the blade surface. This cooler air is supplied through internal serpentine passages that are cast in the blade during the manufacturing process. The air that flows in the passages is also used to remove heat that conducts through the blade wall from the hot external surface. Thus, increasing the heat transfer in the serpentine passages is desirable. Depending on the location of the serpentine passage, different heat transfer enhancement schemes are used. In the passage near the trailing edge, it is common to use pin fins, dimples, ribs or a combination of these. For the passages in the mid portion and near the leading edge, ribs are typically used. In the leading edge passage, jet impingement on the curved surface helps to reduce the blade surface temperature. These heat transfer enhancement techniques are discussed in depth by Han et al. [1].

Of interest in the current study is the heat transfer associated with ribs in internal serpentine passages. Ribs help to increase heat transfer by breaking the hydrodynamic boundary layer that forms due to viscous effects. There are also other important characteristics that are associated with ribbed channel flow that will be discussed later. Over the years, studies have been performed to investigate different factors that impact the level of heat transfer in ribbed channels. Some of the factors that have been identified are channel aspect ratio (*AR*), rib configuration (P/e, e/H, e/D_h, α), rotation number (*Ro*), and channel entrance effects.

The channel aspect ratio in the current study is defined as the ratio of the channel width (W) to the channel height (H) or $AR = W:H$ equivalently $AR = W/H$. Channels that are narrow (AR = 1:4 and 1:2) are more representative of cooling channels near the leading edge portion of the gas turbine blade as shown in Fig. 1. In the narrow channels, the leading (suction side) and trailing (pressure side) walls are far apart. In the middle portion of the blade, the channels tend to be more square and channels with AR = 1:1 are used to study the flow and heat transfer for this portion of the blade. Wide aspect ratio channels (AR = 2:1 and 4:1) are used to simulate internal passages near the trailing edge of the blade. In the wide aspect ratio channels, the leading and trailing walls are closer to each other. Most of the studies that have been performed focus on the leading and trailing walls because these tend to have greatest need for increased heat transfer. An inquisitive thought that arises from the above statements about the channel aspect ratio is what will be the impact of the aspect ratio on heat transfer. It is expected that heat transfer will be different for each aspect ratio because the flow field will be dependent on the channel geometry. In fact this is just what previous research has shown. Furthermore, by introducing ribs onto the walls of stationary channels, the flow field becomes more complicated. Finally, when rotating, the flow field is further increased in complexity. Some important questions that early researchers investigated were; what angle of the rib relative to the mainstream flow will

* Corresponding author.
E-mail address: jc-han@tamu.edu (M. Huh).

0017-9310/$ - see front matter © 2009 Elsevier Ltd. All rights reserved.
doi:10.1016/j.ijheatmasstransfer.2009.03.021

Nomenclature

A	area
AR	aspect ratio
Bo	buoyancy parameter
c	specific heat at constant pressure
D	diameter
e	rib height
H	channel height
h	regionally averaged heat transfer coefficient
i	designates a given region in the channel ($1 \leqslant i \leqslant 12$)
I	current
k	thermal conductivity of the air
m	mass flow rate
Nu	Nusselt number
P	rib pitch
Pr	Prandtl number of the air
Q	heat transfer
R	radius of rotation
Re	Reynolds number
Ro	Rotation number
T	temperature
U	velocity in streamwise direction
V	voltage
W	channel width

Greek symbols

α	rib angle with respect to mainstream flow direction
β	angle of channel orientation with respect to the axis of rotation
μ	viscosity of air
ρ	density of air
Ω	rotational speed

Subscripts

t	total
p	projected
h	hydraulic
htr	heater
x	local
o	fully developed turbulent flow in non-rotating smooth pipe
s	stationary
n	net
l	loss
w	wall
b	bulk
f	film
in	inlet
e	exit

result in highest heat transfer? How far should the ribs be placed apart? What is the impact of rib height on the heat transfer? How will the pressure drop in the channel be affected by the ribs? What effects does rotation have on the heat transfer? As can be expected all of these parameters will be dependent on the aspect ratio of the channel.

1.1. Aspect ratio effects (stationary)

To answer some of the questions just posed, early studies investigated heat transfer in stationary channels. By doing so, valuable insight was gained in how the ribs and channel aspect ratio affect the flow field and heat transfer. Han [2] investigated the effect of the channel aspect ratio on heat transfer for five different channel aspect ratios (AR = 1:4, 1:2, 1:1, 2:1, 4:1) with traverse ribs ($\alpha = 90°$). He showed that for the same rib configuration (e/D_h, P/e) the local heat transfer in the wide aspect ratio channel (AR = 2:1 and 4:1) is higher than the narrow aspect ratio channel (AR = 1:4 and 1:2). Han and Park [3] investigated the heat transfer performance in channels of different aspect ratios with angled ribs. The heat transfer performance takes pressure drop into consideration along with heat transfer levels. Their study considered rectangular channels with AR = 1:1, 2:1, and 4:1. They showed that the heat transfer performance increases by using angled ribs. However, the increase in heat transfer performance is strongly dependent on the aspect ratio of the channel. The square channel in their study showed a larger increase in heat transfer performance than the wide aspect ratio channels (AR = 2:1 and AR = 4:1). Afterwards, Park et al. [4] expanded the study to include other aspect ratios (AR = 1:4, 1:2, 1:1, 2:1, and 4:1). The results showed that narrow aspect ratio channels (AR = 1:4 and 1:2) have better heat transfer performance than wide aspect ratio channels (AR = 2:1 and 4:1). From these studies just cited, it is clear that the aspect ratio of the channel plays an important role on the heat transfer and pressure drop in the channel. Conclusively, these studies showed that the discoveries made for one particular aspect ratio may not carry over to a different aspect ratio channel. Since most studies have focused on square and wide aspect ratio channels, a narrow aspect ratio channel of 1:4 was chosen for this investigation.

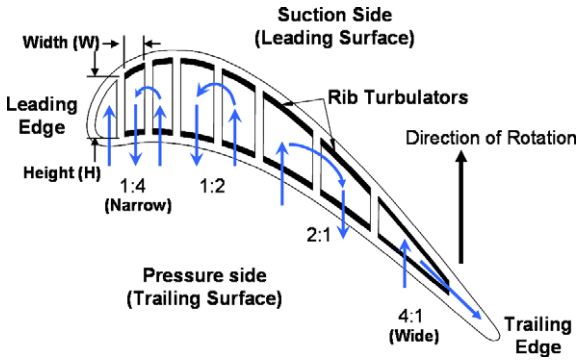

Fig. 1. Gas turbine blade internal cooling channels and their applicable aspect ratios.

1.2. Rib configuration effects (stationary)

In the studies mentioned previously, the main focus was on the aspect ratio in ribbed channels. However, all of the studies mentioned previously also paid attention to rib configuration. Rib configuration, be it rib spacing, blockage ratio, rib angle etc., has a tremendous influence on the heat transfer and pressure drop. In the same study that Han [2] performed, the blockage ratios (e/D_h) tested were 0.047 and 0.078 with rib pitch to rib height ratios of P/e = 10 and P/e = 20. He discovered that the local heat transfer enhancement on the ribbed wall decreased with increasing P/e. Likewise, Han and Park [3] included the effects of rib angle in their study. In that study, the ribs were placed at various angles with P/e = 10 and 20. They concluded that the heat transfer performance can be increased if angled ribs are used instead of traverse ribs. For example, in their study, the square channel with angled ribs had a 30% higher heat transfer performance than the traverse rib case. Park et al. [4] studied rib angles of 90°, 60°, 45°, and 30°. All cases considered ribs with P/e = 10 and blockage ratios of e/D_h = 0.047 and 0.078. For the

square channel and the narrow aspect ratio channels, the ribs with a 60°/45° angle had higher heat transfer performance. The wide aspect ratio channels gave the best heat transfer performance with ribs at angles of 45°/30°. Han et al. [5] studied the effects of rib spacing in a wide aspect ratio channel of 12:1. They measured heat transfer and pressure drop for P/e = 5, 7.5, 10, 15 and 20. The blockage ratios (e/D_h) were also varied from e/D_h = 0.032 to 0.102. Their results showed that for traverse ribs, the best heat transfer performance occurred for P/e = 10. They also discovered that as the blockage ratio increases, the friction factor increases. Taslim and Spring [6] used a liquid crystal technique to investigate the effects of rib profile, rib spacing, and blockage ratios on heat transfer and friction. The tests that they performed considered P/e ratios ranging from 4.27 to 10, with multiple P/e ratios in between. The blockage ratios ranged from e/D_h = 0.15 to 0.285. From their experiments, they found that the optimum P/e ratio is dependent on the blockage ratio and channel aspect ratio. They also pointed out that the heat transfer becomes less dependent on the rib spacing as the blockage ratio decreases. Han [7] investigated rib spacing and blockage ratio effects in a square channel with P/e = 10, 20, and 40. The blockage ratios he tested were e/D_h = 0.021, 0.042, and 0.063. For a rib spacing of P/e = 10 he discovered that as the blockage ratio increases, the friction factor and the Stanton number both increase. Furthermore, he showed that for a blockage ratio of e/D_h = 0.063, the average friction factor and Stanton number decreased with increasing P/e. In a recent study by Huh et al. [8], the effect of rib spacing was studied in a 1:4 aspect ratio channel. The rib pitch to rib height ratios studied were P/e = 2.5, 5, and 10 with a constant blockage ratio of e/D_h = 0.078. That study showed that the P/e = 10 case provided the best heat transfer. Clearly, previous studies showed a dependence of the heat transfer on the aspect ratio. However, for the 1:4 channel this influence of the blockage ratio has not been reported. The current study will add to Huh et al. [8] by evaluating a blockage ratio two times as large.

1.3. Rotation number effects

One drawback to the stationary experiments is that the effects of the Coriolis and rotation induced buoyancy forces, which occur under rotating conditions in a heated channel, are not present. The flow field is strongly affected by rotation and thereby the heat transfer. To quantify the effect of rotation, the ratio of the Coriolis force to the flow inertial force is considered. This ratio is referred to as the rotation number (Ro). Guidez [9] experimentally studied the convective heat transfer in a rectangular rotating channel. He theoretically analyzed rotation effects with a 3D Navier–Stokes turbulant mixing length model. He concluded that Coriolis acceleration has a beneficial influence on the mean heat transfer. Wagner et al. [10,11] performed experiments in a smooth walled square channel with both radially outward and radially inward flow in a multi-pass model. The rotation number for their tests ranged from 0.0 to 0.48. Their results showed that an increase in the rotation number will cause the heat transfer to increase on the trailing surface and to decrease on the leading surface for a radially outward flow condition. For the radially inward flow case, the leading surface heat transfer was not affected greatly. The trailing surface heat transfer is strongly impacted by the flow direction. Taslim et al. [12] performed experimental heat transfer testing using a liquid crystal technique. They studied the rotation effects in channels with ribbed walls. The rotation number for their tests ranged from 0.0 to 0.3. They noted that as the rotation number increased, the heat transfer also increased on the trailing surface. On the leading surface, the heat transfer decreased with an increase in rotation number. Azad et al. [13] and Al-Hadhrami et al. [14] performed rotating experiments in a 2:1 ribbed channel with rotation numbers ranging from 0.0 to 0.21. The results from Azad et al. [13] and Al-Hadhrami et al. [14] confirmed the results of Wagner et al. [10,11] and Taslim et al. [12]. Fu et al. [15] performed experiments in ribbed channels with narrow aspect ratios. The rotation number in their study ranged from 0.0 to 0.3. They concluded that the heat transfer was strongly dependent on rotation on the first pass leading wall with radially outward flow. This result is different from the wide aspect ratio channels where the rotation had a weak impact on the leading wall in the first pass.

1.4. Entrance effects

Numerous studies have focused on internal heat transfer in rotating channels under fully developed flow conditions. However, the internal flow channel of the gas turbine blade in engines experiences strong effects due to the entrance geometry. The heat transfer enhancement differs from that of fully developed flow when entrance effects are present. Wright et al. [16] conducted a survey of rectangular channels with aspect ratios of 4:1 and 8:1. They studied three different entrance geometries and concluded that the entrance effects will greatly enhance the heat transfer. They showed that as the rotation number increases, the effect of the entrance geometry decreases. They also showed that the influence of the entrance geometry on the heat transfer is more apparent in the smooth channels than in the ribbed channels. More recently, Liu et al. [17] investigated heat transfer at high rotation numbers of 0–0.65 in a narrow aspect ratio channel of 1:4. The entrance condition for that study was a sharp bend. This entrance geometry resulted in high heat transfer in the channel first pass compared to a fully developed case of Fu et al. [15]. The sharp entrance condition also reduced the effect of rotation in the first passage. In the second pass, the entrance geometry had little effect due to the strong turn effect.

1.5. Objectives

From the brief review of previous work, it is clear that there are a variety of factors that ultimately dictate the heat transfer in the gas turbine blade. This study was undertaken because of the limited amount of information for ribbed 1:4 channels with an entrance condition that is in the developing state. None of the studies cited provide information for blockage ratio effects in rotating narrow aspect ratio channels. It is not yet clear if using a tall rib will affect the Coriolis and buoyancy forces in rotating channels. This study aims to provide an insight on the:

1. Effect of the blockage ratio on rotation in a narrow channel.
2. Heat transfer characteristics for a ribbed 1:4 aspect ratio channel with a blockage ratio of 0.156 at high rotation numbers.
3. Interaction between the entrance geometry and rotation.
4. Effect of adjacent ribbed walls on the tip cap heat transfer trends.
5. Correlation of heat transfer enhancement due to rotation with the buoyancy parameter in an extended range up to 1.5 (Ro = 0.65).

2. Experimental setup

In a gas turbine, the rotational speed can be several thousand rpm. This rotation causes drastic changes in the internal cooling passage flow field when compared to a stationary channel because of the rotational induced buoyancy and Coriolis forces. To quantify these effects, the ratio of the Coriolis force to the bulk inertia force of the flowing fluid is considered by the rotation number. Typical rotation numbers for real aircraft engines are near 0.25 with Reynolds numbers in the range of 50,000. Reaching several thousand rpm in rotating experiments in a laboratory setting is quite difficult. However, by considering the rotation number, real engine conditions can be simulated in a laboratory. One method to achieve

similar conditions for the large real engine rotation number in the laboratory is to use air at high pressure. As the pressure of the air increases so will the density. For a fixed mass flow rate (Reynolds number) and hydraulic diameter, an increase in density will result in a decrease in velocity. A lower velocity will in turn increase the rotation number. In order to achieve larger rotation numbers at higher Reynolds numbers, the experiments for the present study were conducted with air at a pressure of 75 psig. For the current study, a rotation number of 0.65 and 0.16 can be achieved at Reynolds numbers of 10,000 and 40,000, respectively. These conditions are approaching the real engine condition.

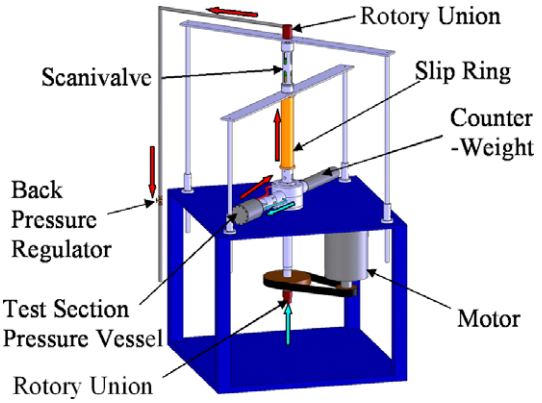

Fig. 2. Rotating arm assembly used to perform heat transfer experiments with the 1:4 aspect ratio test section.

2.1. Rotating facility

Fig. 2 shows the rotating arm assembly used to conduct the experiments for the current study. A steel table is used as the support structure. A 25 hp electric motor is used to drive the shaft which spins the arm. Counterweights, located opposite of the test section pressure vessel, are used to balance the arm so that minimal vibrations are experienced during rotation. Air from a compressor enters an ASME square-edge orifice meter (not shown) where the mass flow rate is measured. Air enters the rotating assembly at the bottom of the shaft via a rotary union. The air then passes through the hub and into the bore of the arm. A rubber hose is used to direct the flow from the arm to the test section housing. After the air flows through the test section, it exits the pressure vessel. The hot exhaust air is then directed, by means of a rubber hose, to the slip ring. A ½-in. copper tube, which passes through the bore of the 100 channel slip ring, is used to direct the air to the top rotary union. Steel pipe is connected to the top rotary union and a valve is used to adjust the back pressure of the system.

2.2. Test section (AR = 1:4)

The channel geometry with a sharp entrance is shown in Fig. 3(a). The air passes through a 9.525 mm inlet hose into the curved plenum region. After direct impingement on the plenum region, the flow is re-directed into the 1:4 aspect ratio test section as shown. A screen was placed prior to the first copper plate region of the test section, to help spread the flow at the entrance. The wire diameter of the screen is 0.015 mm. A nylon substrate, with a low thermal conductivity, is used to support the copper plates

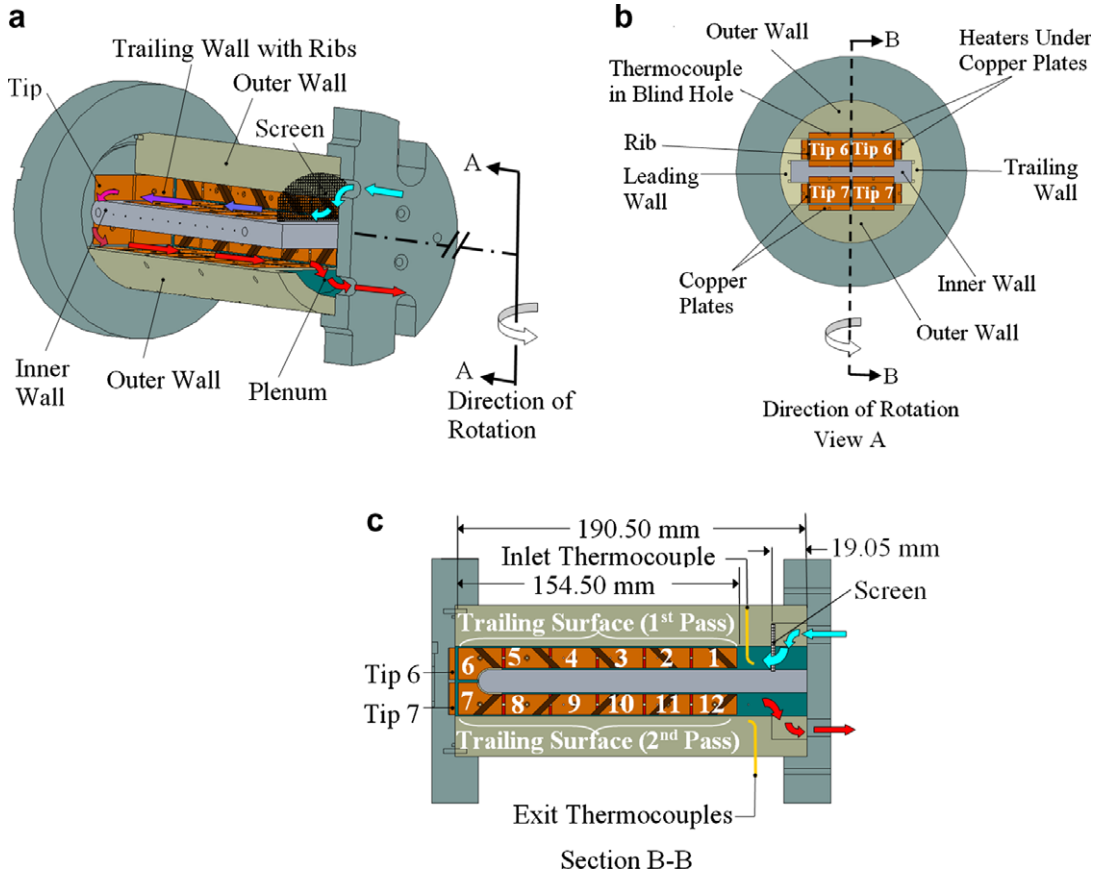

Fig. 3. (a) Drawing showing the flow channel geometry of the 1:4 aspect ratio test section (b) test section tip view showing location of heaters and wall naming convention (c) test section view showing the copper plate region numbering convention.

and heaters. Between each copper plate is a strip of insulation material which prevents conduction between copper plates and also helps to create a smooth surface between adjacent copper plates.

As the air passes through the test section, it is heated using prefabricated silicone rubber heaters that are placed beneath the copper plates as can be seen in Fig. 3(b). A total of 12 heaters are used for the outer, inner, leading and trailing walls. An additional heater is used for the tip. Thermally conductive paste is used between the heaters and the copper plates in order to reduce contact resistance. Blind holes, with a diameter of 1.59 mm, are drilled 1.59 mm deep on the backside of each copper plate. Thermocouples are placed inside of the blind holes of the copper plates and are affixed to the copper plates using highly conductive epoxy. Fig. 3(c) shows that each passage is divided into six regions. There are a total of twelve regions in the test section. The overall test section length is 190.50 mm. The heated channel length of each passage is 154.50 mm and the plenum length is 19.05 mm.

The slip ring used in the experiments consisted of 100 channels. Each heater and thermocouple required two channels (positive and negative). Thus, a total of 26 channels were needed for the 13 heaters. Temperature measurements from the 24 thermocouples placed inside the leading and trailing copper plate blind holes utilized an additional 48 channels. The tip cap region consisted of four copper plates, and as such, required four thermocouples that utilized 8 slip ring channels. In regions 4 and 10, temperature measurements were taken on the outer-leading, outer-trailing, inner-leading, and inner trailing surfaces. This resulted in using 8 thermocouples that utilized 16 slip ring channels. Thus, overall, a total of 34 temperature measurements were made from the copper plates in the channel. Furthermore, one thermocouple is placed at the inlet to measure the air temperature as it enters the test section. At the exit of the test section, two thermocouples are used to measure the air temperature. Thus, a total of 6 slip ring channels were needed for air temperature measurements.

The thickness of all copper plates is 3.175 mm. The copper plates on the leading and trailing walls are rectangular in shape and measure 23.81 mm × 11.11 mm. The outer and inner wall copper plates are square and measure 23.81 mm × 23.81 mm. The tip copper plates are rectangular with dimensions of 23.81 mm × 17.46 mm. The flow channel width is 50.8 mm and has a height of 12.70 mm, resulting in a hydraulic diameter (D_h) of 20.32 mm. The test section consists of two passes. The flow in the first passage is radially outward, and after a 180° turn, the flow is radially inward.

Fig. 4 shows details of the rib roughened surface of the test section. Ribs were placed on the leading and trailing walls of both passes in a parallel configuration. For the e/D_h = 0.156 case, the ribs have a square cross-section measuring 3.175 mm × 3.175 mm and are made of brass. Similarly, the ribs have for the e/D_h = 0.078 case, also have a square cross-section with measurements of 1.59 mm × 1.59 mm. A very thin layer of thermally conductive glue is used to affix the ribs to the surface of the copper plates. The ribs are placed at a 45° angle relative to the mainstream flow.

For the present study, the test section was oriented 90° to the direction of rotation. The rib pitch-to-rib height (P/e) ratio was held constant at 10. The air pressure was maintained at 75 psig for all cases studied. The Reynolds numbers tested were 10,000, 15,000, 20,000, 30,000, and 40,000. At each Reynolds number, the rotational speed was varied from 0 to 400 rpm with an increment of 100 rpm.

2.3. Data acquisition system

Signals from the 37 thermocouples that were installed in the test section, pass through the 100 channel slip ring. The thermocouple wires from the slip ring stationary side are connected to two 32 channel (National Instruments) NI SCXI-1303 modules. These modules are coupled with two 32 channel NI SCXI-1102 thermocouple amplifiers that are housed in NI SCXI-1000 chassis. The chassis passes data to a LabView program where temperature measurements are displayed. The program collects data at a rate of 100 scans/s. Temperatures are recorded when steady state is achieved. Steady state is considered to have been reached once all temperature changes are less than 0.5 °C per hour.

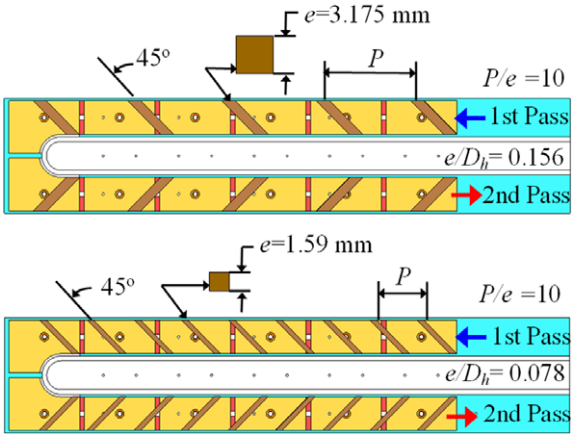

Fig. 4. Drawing showing the rib configurations for the current study (P/e = 10, e/Dh = 0.156) and Huh et al. [8] (P/e = 10, e/Dh = 0.078).

3. Data reduction

3.1. Heat transfer enhancement

This study investigates the regionally averaged heat transfer coefficient (h) at various locations within a rotating duct. A uniform wall temperature of 65 °C, in the circumferential direction, is maintained at regions 4 and 10 throughout all the tests. The density ratio, based on the uniform wall temperature (65 °C) and the temperature of the air at the inlet (23 °C) is 0.11. In the current study, the regionally averaged heat transfer coefficient is calculated using the net heat transferred to the air from the heated copper plate (Q_n), the total heat transfer surface area (A_t = smooth area between ribs plus the area of 3 rib sides) at each region, the local region wall temperature of the plate ($T_{w,x}$), and the local bulk mean temperature of the air flow in the channel ($T_{b,x}$). Therefore, the regionally averaged heat transfer coefficient is given as

$$h = (Q_n/A_t)/(T_{w,x} - T_{b,x}) \quad (1)$$

The net heat transfer is calculated as:

$$Q_n = (V \cdot I)(A_p/A_{htr}) - Q_l \quad (2)$$

The voltage (V) is measured with a multi-meter and the current (I) is supplied to each heater by variac transformers. The power input to each heater is multiplied by the ratio of the projected heat transfer area (A_p) to the total heater area (A_{htr}). In order to determine the external heat losses (Q_l) escaping from the test section during the experiment, two heat loss calibration tests are performed. The first heat loss calibration test is performed at a lower wall temperature than the experiment wall temperature. Similarly, a second heat loss calibration test is performed at a higher wall temperature than the experiment wall temperature. During the heat loss calibration tests, the wall temperature is maintained by supplying power to each heater with the variac transformers. A successful heat loss calibration test is achieved when the total power input to the test section reaches equilibrium with the environment (i.e. the wall temperature reaches a steady state condition). The heat loss which occurs

during the experiment is then determined by interpolating between the two sets of heat loss data. It is noted that heat loss calibration tests were performed at all rotational speed conditions considered in the present study and the stationary case as well. In order to minimize natural convection effects during the heat loss calibration tests, an insulating material was placed inside of the flow channel.

The local regional wall temperature ($T_{w,x}$) is directly measured using the thermocouple installed in the blind hole on the backside of each copper plate. Because the plates are made of copper, which has a high thermal conductivity, the temperature of each plate is assumed uniform. One thermocouple at the inlet and two thermocouples at the outlet of the test section measure the inlet and outlet bulk temperatures, respectively. Therefore, the local bulk air temperature at any location in the test section can be calculated using linear interpolation. The results presented in this study are based on the linear interpolation method. Although linear interpolation was chosen for determining the air temperature at various locations in the channel, the bulk air temperature can also be calculated using the conservation of energy principle. For the present study, both methods compare very well. To determine the bulk air temperature by an energy balance, Eq. (3) can be used. Thus, for a given region i ($1 \leqslant i \leqslant 12$) the energy balance equation is:

$$(T_{b,e} - T_{b,in})_i = \sum_i Q_n/(m \cdot c) \tag{3}$$

In Eq. (3), $T_{b,in}$ is the bulk air temperature at the inlet of region i and $T_{b,e}$ is the bulk air temperature at the exit of region i. The net heat transferred to the air, from all four surfaces (leading, trailing, inner, and outer walls) at region i, is divided by the product of the mass flow rate (m) and the specific heat at constant pressure (c). Thus, for the first region at the channel inlet (region $i = 1$), $T_{b,in}$ is the actual measured temperature of the air using the channel inlet thermocouple. Heat is added to the air in region $i = 1$ from all four walls. This results in a bulk air temperature increase at the exit of region $i = 1$. At the exit of region $i = 1$, the bulk air temperature is $T_{b,e}$ which is also the inlet temperature for region $i = 2$. The local bulk air temperature $T_{b,x}$ in region i is then determined as the average of $T_{b,in}$ and $T_{b,e}$.

The Dittus–Boelter/McAdams correlation for heating ($T_{w,x} > T_{b,x}$) is used in this study to provide a basis of comparison. The Dittus–Boelter/McAdams correlation is used to calculate the Nusselt number (Nu_o) for fully developed turbulent flow through a smooth stationary pipe. Therefore, the heat transfer enhancement (Nu/Nu_o ratio) is given as:

$$(Nu/Nu_o) = [(h \cdot D_h)/k][1/(0.023 \cdot Re^{0.8} \cdot Pr^{0.4})] \tag{4}$$

where h is calculated by Eq. (1). All air properties are taken based on the channel average bulk air temperature with a Prandtl number (Pr) for air of 0.71.

3.2. Experimental uncertainty

An uncertainty analysis was performed based on the method described by Kline and McClintock [18]. The estimated uncertainty for the temperature instrumentation is 0.5 °C. The uncertainty of the Nu/Nu_o ratio is approximately 6% for the highest Reynolds number. For the lowest Reynolds number (Re = 10,000), the maximum uncertainty is approximately 7.1%.

4. Discussion of results

4.1. Flow field behavior

Before discussing the experimental results for the two pass 1:4 aspect ratio channel with angled ribs, it is necessary to understand the flow behavior inside the ribbed channel. Fig. 5 presents conceptual views of the most notable characteristics of the effects of angled ribs on the mainstream flow. Theses effects are: mainstream flow separation, recirculation, reattachment, turbulent mixing, and angled secondary flow. As shown in Fig. 5(a), as the mainstream flow near the wall of the channel passes over the rib, it separates from the wall due to the rib. This separation results in relatively low heat transfer just downstream of the rib, due to a relatively hot cell being trapped in the area of recirculation. However, when the mainstream flow reattaches to the wall (between two ribs), this is an area of relatively high heat transfer due to impingement of the mainstream flow on the surface. Redevelopment of the boundary layer then begins. This pattern of separation, recirculation, and reattachment continues throughout the channel along with the pattern of repeating ribs. In addition to general flow separation and reattachment, the rib turbulators increase turbulent mixing. The relatively hot fluid near the surface is continuously mixing with the relatively cooler core fluid near the center of the channel. This mixing also serves to increase the heat transfer from the channel wall.

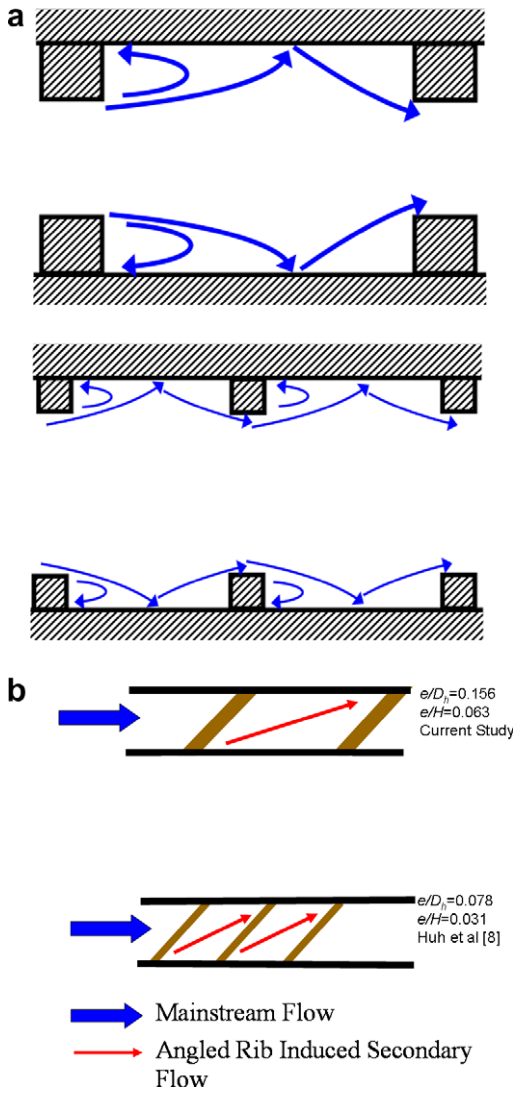

Fig. 5. Effect of rib on (a) mainstream flow separation and reattachment and (b) angled secondary flow.

The orientation of the rib turbulators has a significant impact on the level of heat transfer enhancement. It has been shown that skewed ribs yield significantly higher heat transfer enhancement than orthogonal ribs. This is due to the additional secondary flow

induced by the angle of the ribs. The fluid near the surface follows the angle of the rib. This angled rib induced secondary flow creates a set of counter-rotating vortices in the channel. The secondary flow follows the rib until it impinges on the side wall as can be seen in Fig. 5(b). After impingement on the side wall, the angled rib induced secondary flow returns to the other side wall, creating a vortex. This behavior is identical on both the leading and trailing surfaces, so two counter rotating vortices form in the channel.

The ratio of rib height (e) to channel height (H) (e/H) also is important. Kim et al. [19] explained that by increasing the ratio, flow is accelerated over the ribs, producing higher heat transfer levels. In that study, the blockage ratio was changed by decreasing the channel height H. The channel hydraulic diameter D_h was kept constant. In the current study, the channel height is kept constant along with the channel hydraulic diameter. The blockage ratio is increased by increasing the rib height (e). What is not clear yet, is if the doubling of the blockage ratio, in the narrow aspect ratio channel, will alter the heat transfer. In the current study, the blockage ratio is twice that of the previously reported study (Huh et al. [8]). It is speculated that the rib height may also alter the size of the angled rib induced counter rotating vortices. For the larger rib height, the vortex might be larger due to the taller ribs. By having larger vortices, more heat can be removed from the hot wall and transferred to the cool mainstream flow.

The level of heat transfer enhancement in the two pass channel with angled ribs is also altered by the sharp 180° turn which connects the first pass to the second pass, by rotation, and by rotational induced buoyancy forces. Fig. 6 shows the secondary flows induced by angled ribs, the 180° turn and rotation. The secondary flow induced by rotation, is a result of the Coriolis force. As conceptually shown in Fig. 6(a), with a 90° channel orientation, the Coriolis force induces a pair of vortices, which circulate toward the trailing wall for radial outward flow (first pass) and toward the leading wall for radial inward flow (second pass). This cross-stream secondary flow pattern significantly increases heat transfer on the trailing wall in the first pass and the leading wall in the second pass. However, the rotation induced secondary flow reduces heat transfer on the leading wall in the first pass and trailing wall in the second pass. In the current study, the secondary flow caused by the 45° angled ribs that are located on the leading and trailing walls in the first pass, cause impingement of the flow onto the outer wall. In the second pass, the secondary flow due to the ribs cause impingement onto the inner wall as is shown in Fig. 6(a).

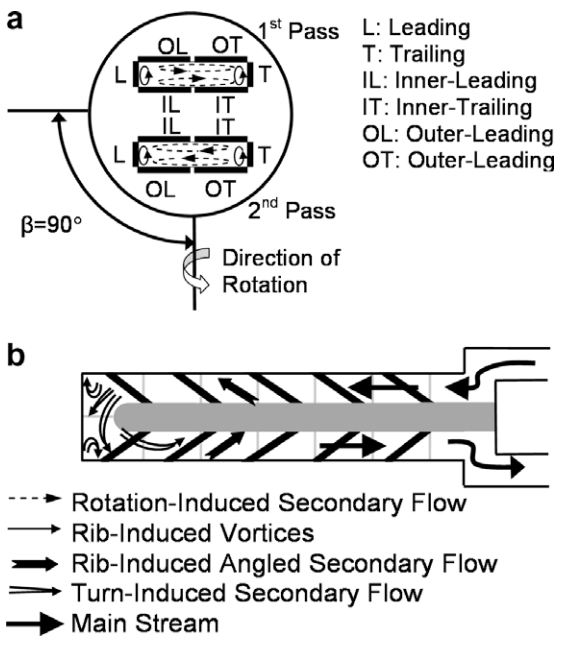

Fig. 6. Conceptual view of (a) rib and rotation induced secondary flow inside a two-passage rectangular channel (AR = 1:4), (b) rib and turn induced secondary flow.

When the mainstream flow passes through the 180° turn, the flow impinges on the outer wall of the second pass, then reattaches on the inner wall in the second pass as is shown in Fig. 6(b). A circulation zone right after the turn near the inner wall in the second pass is created due to the sharp turn. Two additional circulation zones occur in the outer corners of the turn because of the geometry. These flow structures, due to the turn, result in different heat transfer enhancements inside the turn and after the turn. All of these secondary flows, induced by angled ribs, the 180° turn, and rotation, interact to make flow through a rib roughened serpentine passage very complex. The combination of these flows may result in further enhancement of the heat transfer, or they may have a negative impact on the heat transfer trend. The flow patterns previously described have been observed by previous studies (Han et al. [20], Han and Zhang [21], Ekkad and Han [22], Park and Lau [23], Park et al. [24], Liou et al. [25], Liou and Chen [26], Liou et al. [27]).

Rotation causes a difference in the heat transfer between the leading and trailing walls as mentioned previously. The effect of rotation is evaluated by the rotation number (Ro). The rotation number is defined as the ratio of the Coriolis force to the inertial force as shown in Eq. (5)

$$Ro = (\Omega D_h)/U_b \tag{5}$$

The combined effect of rotation and temperature difference is evaluated by the local buoyancy parameter (Bo_x). For the radial outward flow in the first pass, the inertial force is in the same direction as the rotation-induced centrifugal force. The rotation induced centrifugal force opposes the inertial force in the second pass because the flow direction is reversed. The buoyancy parameter, as defined by Wagner et al. [10], is used to present the combined effects of the Coriolis and rotation induced buoyancy forces.

$$Bo_x = (\Delta\rho/\rho_{b,x})(Ro)^2(R_x/D_h) \tag{6}$$

This local buoyancy parameter can be re-written by incorporating the measured wall and bulk air temperatures as shown in Eq. (7).

$$Bo_x = [(T_{w,x} - T_{b,x})/T_{w,x}](Ro)^2(R_x/D_h) \tag{7}$$

In the current study, to more accurately determine the local buoyancy parameter, the local wall temperature in the denominator of Eq. (7) is replaced by the local film temperature ($T_{f,x}$). The local film temperature is the average of the local wall and the local bulk temperatures as shown in Eq. (8).

$$T_{f,x} = (T_{w,x} + T_{b,x})/2 \tag{8}$$

4.2. Streamwise Nu ratio distribution results-stationary

When the channel is not rotating, the flow complexity is reduced because of the absence of the Coriolis force and rotational buoyancy effect. However, the rib effects are still present. These effects were previously stated to be mainstream flow separation, recirculation, reattachment, turbulent mixing, and angled secondary flow. To investigate the effects of the ribs on heat transfer in the stationary channel, the current study is compared to the smooth results of Liu et al. [17] in Fig. 7. The stationary Nusselt number (Nu_s) is normalized by the Nusselt number for smooth, fully developed, stationary round pipe (Nu_o). From this figure, a few important observations are made.

One point to focus on is the effect of the ribs on the entrance effect. The heat transfer is greatly enhanced by the strong entrance condition for both the smooth case and the ribbed case. This is seen

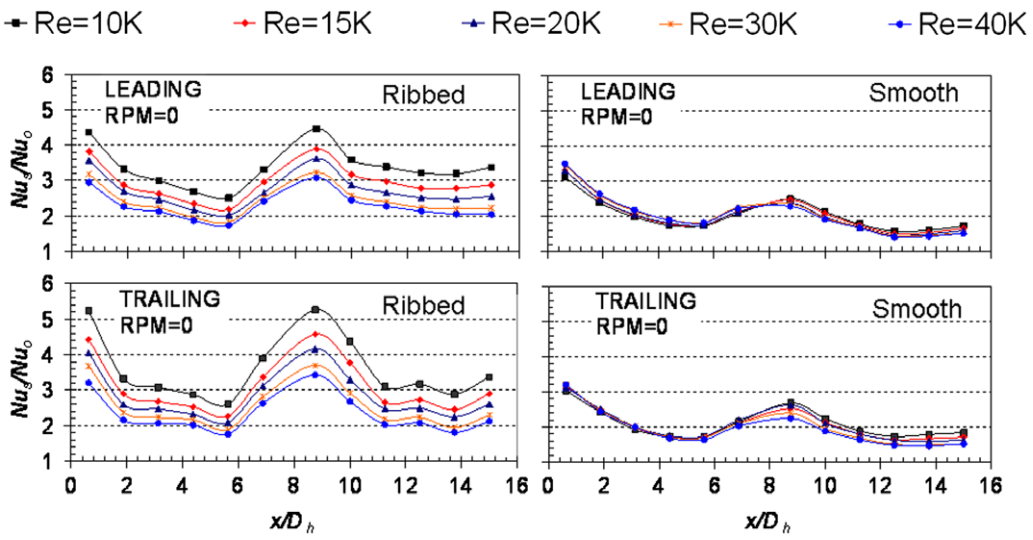

Fig. 7. Stationary streamwise *Nu* ratio (*NuS/Nuo*) distribution for the leading and trailing wall at different Reynolds numbers for the current study (P/e = 10, e/Dh = 0.156) and Liu et al. [17] (smooth).

by the large Nu_s/Nu_o ratios for x/D_h = 0.625. These high Nu_s/Nu_o ratios are a result of a very thin boundary layer and high entrance velocity. For the ribbed case, the Nu_s/Nu_o ratios quickly drop off, and between x/D_h = 1.875 and x/D_h = 4.375, the Nu_s/Nu_o ratios, for a given Reynolds number, remain almost constant for the trailing surface and only slightly decrease for the leading. The behavior for the ribbed case is due to the periodically developing boundary layer. The smooth case is quite different in that the Nu_s/Nu_o ratios continually decrease until x/D_h = 4.375. From these observations one can conclude that the effect of the entrance is more apparent in the smooth channel. Another interesting observation is the large effect of the Reynolds number on the Nu_s/Nu_o ratios for the ribbed case. As the Reynolds number increases, the heat transfer enhancement (Nu_s/Nu_o) continually decreases. However, it is noted that the Nusselt number (Nu_s) actually increases with increasing Reynolds number.

In the turn portion of the channel, the Nu_s/Nu_o ratios are high due to the turn effect. The flow is also increasing in turbulence in the turn portion as described by Liou and Chen [28]. In their 1.25 aspect ratio channel the turbulent kinetic energy increased from 1% in the region prior to the turn to 24% just after the turn in the second pass. The Nu_s/Nu_o ratios for the ribbed case are clearly greater than the smooth channel in the turn region. In the second pass, when x/D_h is greater than (or equal to) 11.25, the Nu_s/Nu_o ratios remain mostly constant for both the ribbed channel and smooth channel, until the exit of the channel is reached at x/D_h = 15. The mostly constant Nu_s/Nu_o ratios are due to the re-development of the boundary layer.

4.3. Streamwise Nu distribution results-rotating

The flow in the heated rotating ribbed channel is quite complex. The Coriolis induced secondary flow along with the rotation induced buoyancy force, combined with the presence of angled rib induced secondary flow, are what make the flow in the channel so interesting. The combined influence on the Nu/Nu_o ratios, from all of the aforementioned effects, is presented in Fig. 8. In this figure, the rotational speed is increased systematically and the

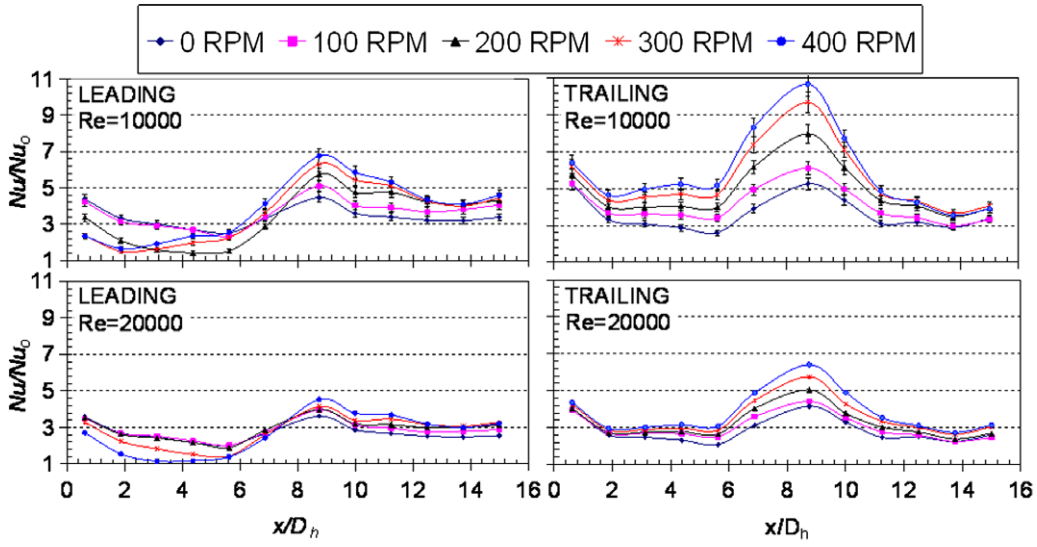

Fig. 8. Streamwise *Nu* ratios (*Nu/Nuo*) distribution at Re = 10,000 and Re = 20,000 for the leading and trailing wall at different rotational speeds for the current study (P/e = 10, e/Dh = 0.156).

streamwise Nu/Nu_o ratio distribution for the leading and trailing surfaces, with ribbed walls, at a Reynolds number of 10,000 and 20,000 is shown.

One observation made immediately is the interesting occurrence on the leading surface, in the first pass ($x/D_h < 6.875$), at a Reynolds number of 10,000. No difference is seen in the Nu/Nu_o ratios for the stationary case and the 100 rpm case. However, for the case of 200 rpm, the Nu/Nu_o ratio is reduced significantly. Furthermore, as the rotational speed is increased to 300 rpm and 400 rpm, an interesting phenomenon occurs. The Nu/Nu_o ratios begin to increase in the streamwise direction for $x/D_h > 1.875$. It is worth noting that at a Reynolds number of 20,000, no decrease is seen in the heat transfer levels until the rotational speed is greater than 300 rpm. Also noted is that the heat transfer levels decrease in the streamwise direction for all rpm.

The trend of the Nu/Nu_o ratios on the trailing surface in the first pass is very different compared to that of the leading surface. For a given x/D_h value, as the rotational speed is increased, (for both Reynolds numbers) the Nu/Nu_o ratios increase. However, this increase is much smaller for the larger Reynolds number case.

In the second pass, for a given x/D_h value greater than or equal to 11.25, at the same Reynolds number and rpm, little difference is seen in the Nu/Nu_o ratios levels between the leading and trailing surfaces. This was not the case for the smooth channel as reported by Liu et al. [17] in which a clear difference was observed.

4.4. Effect of rotation number

The rotation number (Ro) is the ratio of the Coriolis force to the bulk inertial force. From the definition of the rotation number, the same rotation number can be reached by various combinations of rotational speed and fluid bulk velocity. It is vital to show that the rotation number holds valid and can be used to predict heat transfer over an extended range. In Fig. 9, the effect of rotation on heat transfer (Nu/Nu_s) is shown as a function of the rotation number in various regions in the first pass and second pass. The stationary Nusselt number (Nu_s) was chosen as the denominator so that the effects of rotation can be clearly visible.

In the first pass, the Coriolis force skews the mainstream flow towards the trailing wall because the flow is radially outward. Thus, higher velocities are experienced near the trailing wall region. The velocity of the fluid near the leading surface is reduced. One observation that stands out is how the Nu/Nu_s ratios on the trailing surface in region 1 are essentially not affected by rotation. This is due to the strong entrance condition which already serves to provide a high level of heat transfer. However, the leading surface in region 1, experiences a severe degradation in heat transfer enhancement levels ($Nu/Nu_s = 0.5$) with an increase in the rotation number. This finding is extremely important for the gas turbine designer. A 50% reduction of heat transfer in the rotating frame is important because so much of the cooling passage design is based upon stationary measurements. In regions 4 and 6, it is clear that the entrance condition is no longer dominating the heat transfer on the trailing surface. Rather, as the rotation number increases, the trailing surface experiences great heat transfer enhancement due to rotation and reach values of around $Nu/Nu_s = 2.0$. The leading surface Nu/Nu_s ratio trend is quite different from the trailing in regions 4 and 6. In region 4, the leading surface Nu/Nu_s ratios decrease to $Nu/Nu_s = 0.5$ with an increase in rotation number until a critical rotation number of 0.3 is reached. The Nu/Nu_s ratios then begin to increase due to the development of large-scale reverse flow cells as reported by Wagner et al. [10,11] and Su et al. [29]. In region 6, the decrease in Nu/Nu_s ratios on the leading surface is not as severe and only slightly falls below the stationary case. This is mostly due to the high turbulent mixing which occurs in the turn portion.

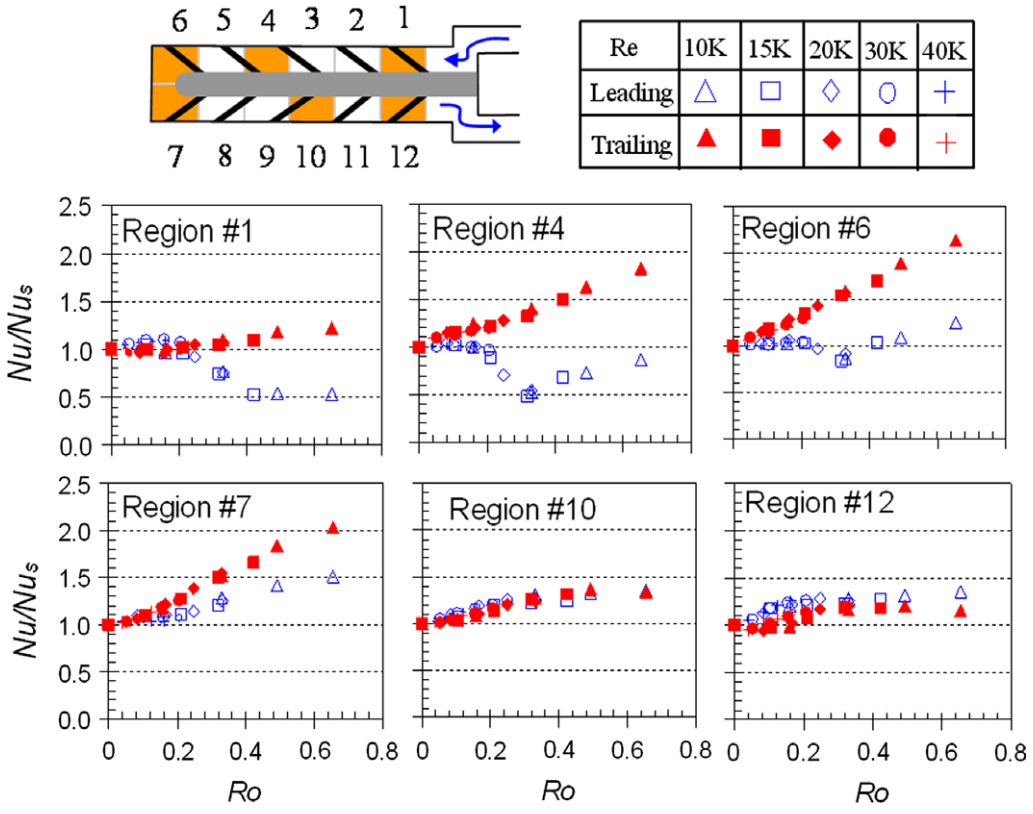

Fig. 9. Regional leading and trailing surface Nu ratios (Nu/Nus) as a function of rotation number (Ro) for the current study ($P/e = 10$, $e/Dh = 0.156$).

In region 7, both the leading and trailing surfaces experience an increase in Nu/Nu_s ratios as the rotation number increases. The trailing surface heat transfer enhancement occurs at a more rapid rate compared to the leading. Little difference is observed in the Nu/Nu_s ratios between the trailing and leading surfaces in region 10. The effect of rotation in this region is reduced and an increase in Nu/Nu_s ratios on both surfaces is about 30% for the highest rotation number reached. When considering these results for gas turbine applications, the reader is reminded that for gas turbines, an increase of 30% in heat transfer is a large amount. In region 12, the Nu/Nu_s ratios on the trailing surface still increase slightly with rotation, but the effect of rotation is even less when compared to region 10. On the leading surface in the region 12, rotation again increases the heat transfer by about 30%. Thus there is little difference between the effect of rotation in region 10 and region 12 on the leading surface.

Although ribs are not placed on the tip cap of the channel, it is interesting to determine how the effects of rotation impact the heat transfer levels in this region. Furthermore, a question that arises is if the adjacent ribbed walls will have an impact on the Nu/Nu_s ratios in the tip region. Fig. 10 compares the heat transfer enhancement due to rotation for two different blockage ratios and the smooth channel condition. From this figure, the effect of rotation seems to be quite similar for all three cases in tip region 6 for both the leading and trailing surfaces. For all three cases, the trailing surface Nu/Nu_s ratios are higher than the leading surface. Also, for all three cases the maximum trailing Nu/Nu_s ratios are 2.25 and the leading Nu/Nu_s ratios are about 1.75–1.85. That is to say, the heat transfer in the rotating frame is about 75–125% of the stationary case. In tip region 7, the smooth channel and the $e/D_h = 0.078$ case again show very similar trends and the effect of rotation is the nearly same for theses two cases. The maximum Nu/Nu_s ratio for the trailing surface in these two cases again reaches to about 2.25–2.4 or nearly 140% of the stationary case. The leading surface maximum Nu/Nu_s ratio for the $e/D_h = 0.078$ case is lower than the smooth case. However, when the blockage ratio is increased to $e/D_h = 0.156$, it is seen that the leading and trailing tip cap surfaces exhibit nearly identical Nu/Nu_s ratios for both the leading and trailing tip cap surfaces. These high Nu/Nu_s ratios in tip region show the gas turbine designer that rotational heat transfer enhancement is large at the tip portion.

4.5. Effect of buoyancy parameter

By heating the walls of the test section, a temperature gradient develops in the fluid from the fluid core to near the wall surface. This temperature gradient results in a variation of the density in the fluid. This density difference and the centrifugal force induced by rotation, result in a rotation induced buoyancy force. The combined effects of temperature and rotation on the heat transfer are realized by investigating how the Nu/Nu_s ratios vary with a change in the buoyancy parameter. In Fig. 11, the effects of the buoyancy parameter on the leading and trailing surfaces Nu/Nu_s ratios in the first pass are shown. The first thing to notice is the behavior of the Nu/Nu_s ratios on the trailing surface. At the entrance (region 1) the heat transfer levels on the trailing surface are only so slightly affected by an increase in the buoyancy parameter. However, notice how the trend of the Nu/Nu_s ratios on the trailing surface becomes more and more dependant on the buoyancy parameter in the streamwise direction. This is ob-

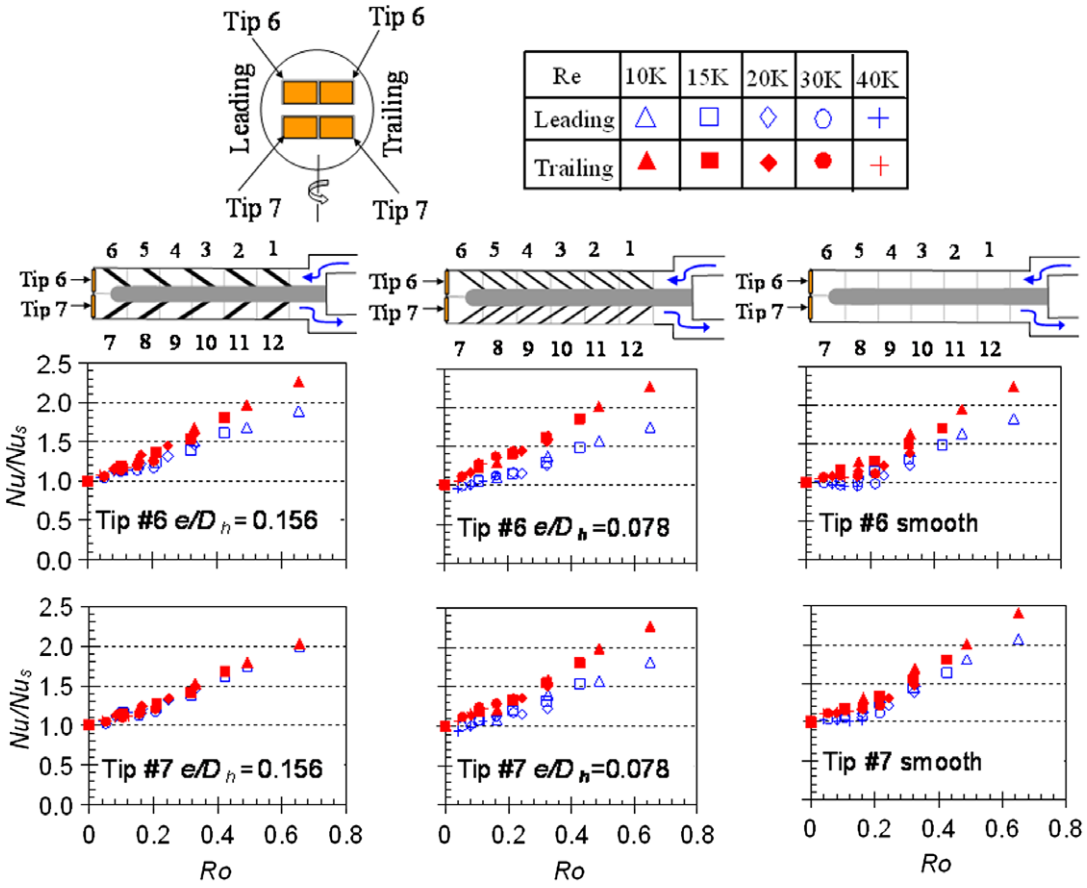

Fig. 10. Comparison of regional tip *Nu* ratios (*Nu/Nus*) as a function of rotation number (*Ro*) for the current study (*P/e* = 10, *e/Dh* = 0.156), Huh et al. [8] (*P/e* = 10, *e/Dh* = 0.078), and Liu et al. [17] (smooth).

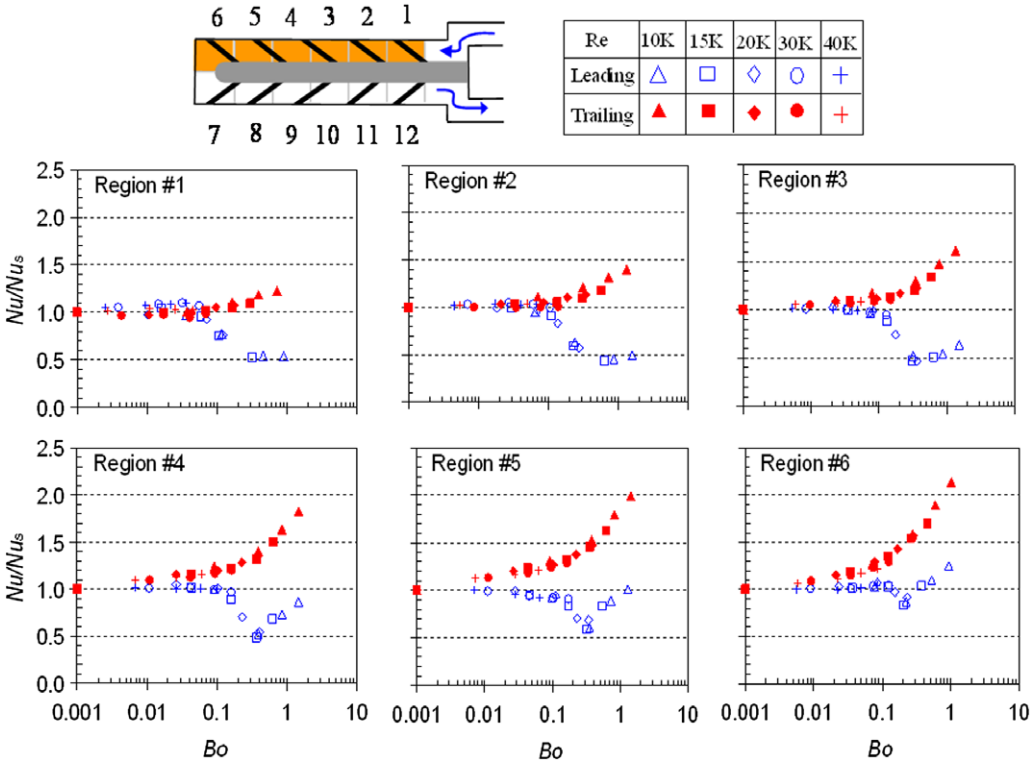

Fig. 11. Regional leading and trailing surface *Nu* ratios (*Nu/Nus*) in the first pass as a function of buoyancy parameter (*Bo*) for the current study (*P/e* = 10, *e/Dh* = 0.156).

served by noticing that an increase in Nu/Nu_s ratios begins to occur at smaller and smaller buoyancy parameter values as you move along in the streamwise direction. The heat transfer on the leading surface also exhibits an interesting behavior. First of all, a decrease in Nu/Nu_s ratios on the leading surface does not occur until a buoyancy parameter value great than 0.1. The Nu/Nu_s ratios on the leading surface decrease to a very low level of 0.5 from region 1 to region 5. That is to say, heat transfer is reduced by 50%, which is significant in gas turbine applications since mostly stationary experimental values are used in gas turbine cooling passage design. In regions 3 through 6, it is seen that a critical buoyancy parameter value is reached ($Bo = 0.2–0.3$) when the Nu/Nu_s ratios begin to increase with an increase of the buoyancy parameter. This is due to the development of large scale reverse flow cells as mentioned previously.

In the second pass of the test section, the mainstream flow direction is reversed. Because the flow is radially inward, the centrifugal force and the inertial force of the flow are counteracting. The velocity profile in the second pass becomes more uniform as compared to the first pass velocity profile. In the first pass, the velocity profile is skewed towards the trailing surface. This is why such a stark difference was observed in heat transfer levels on the leading and trailing surfaces. With this in mind, it is expected that there would not be such a stark contrast in Nu/Nu_s ratios between the leading and trailing surfaces in the second pass, especially after the turn region. In fact, this is the case as seen in Fig. 12. In this figure, the second pass regional heat transfer enhancement levels on the leading and trailing surfaces are shown as a function of the buoyancy parameter. The first thing that is noticed is that indeed in the turn portion (region 7), a noticeable difference in Nu/Nu_s ratios is seen between the leading and trailing surfaces. Both the leading and trailing surfaces increase in heat transfer with an increase in the buoyancy parameter. The increase is greater on the trailing surface with Nu/Nu_s ratios of about 2.0, compared to Nu/Nu_s ratios of 1.5 for the leading surface. This is not to be misunderstood as insignificant since an increase of 50% to 100% is large for gas turbine applications. However, moving along in the steamwise direction downstream from turn, clearly the difference between the leading and trailing surface Nu/Nu_s ratios becomes less and less. From region 7 through region 9, the leading surface Nu/Nu_s ratios remain constant at approximately 1.5 at the maximum buoyancy parameter value of 1.5. On the other hand, the trailing Nu/Nu_s ratios show a continual decrease from region 7 ($Nu/Nu_s = 2.0$) through region 9 ($Nu/Nu_s = 1.5$), at which point both the leading and trailing surface exhibit nearly identical levels of Nu/Nu_s ratios. In regions 10 through 12, the leading surface Nu/Nu_s ratios have fallen to about 1.25 at the maximum buoyancy parameter value. The trailing surface Nu/Nu_s ratios continue to drop from region 10 through region 12. In region 12, the Nu/Nu_s ratios of the trailing surface have fallen below the leading surface Nu/Nu_s ratios; albeit, the difference is small.

One important distinction to make about the heat transfer in the second pass for both the leading and trailing surfaces is that at no point does rotation reduce heat transfer. Rather, rotation is always increasing heat transfer over the stationary case. Whereas, in the first pass, the leading surface heat transfer was reduced by 50% and the trailing surface heat transfer was doubled due to rotation in certain regions.

4.6. Buoyancy parameter correlations

It is advantageous for designers of gas turbine blades to have a trustworthy method by which the internal heat transfer in rotating blades can be predicted within an acceptable margin of error. The buoyancy parameter has been the preferred method to predict heat transfer levels for rotating conditions. However, to fully depend on the buoyancy parameter, it must be shown that this parameter is not limited to only a small range of values and that it is applicable to smooth and ribbed channels. For this reason, the buoyancy parameter has been extended into a larger domain in this study.

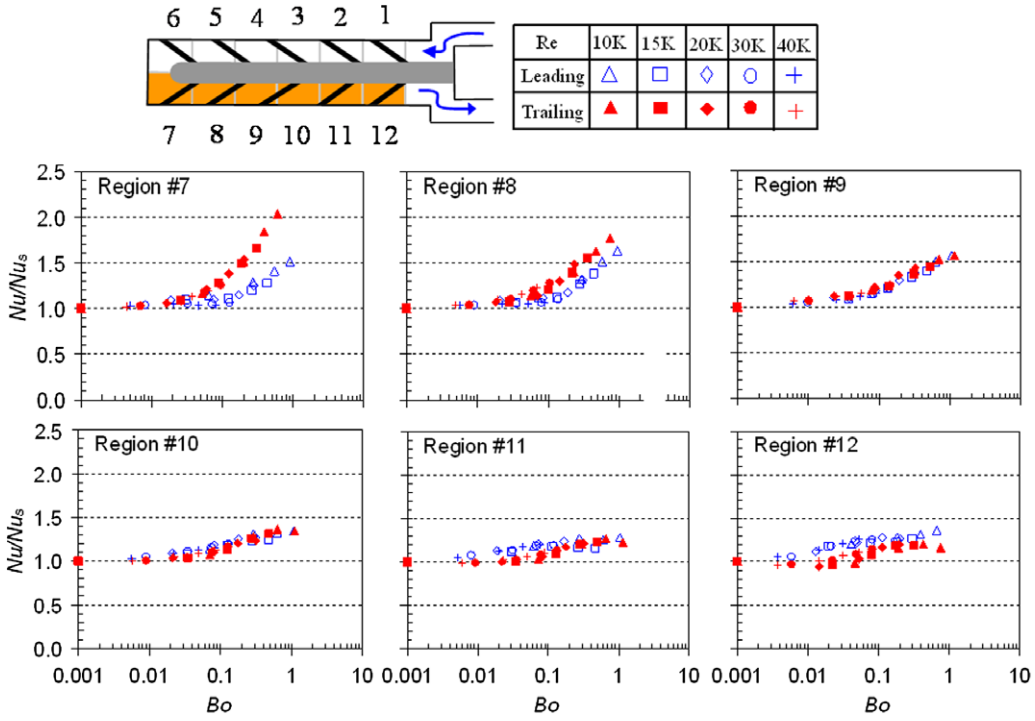

Fig. 12. Regional leading and trailing surface *Nu* ratios (*Nu/Nus*) in the second pass as a function of buoyancy parameter (*Bo*) for the current study (*P/e* = 10, *e/Dh* = 0.156).

The maximum buoyancy parameter reached in this study was *Bo* = 1.5. Not only was the range of the buoyancy parameter extended, but to prove that this parameter is useful to predict the effect of rotation on heat transfer, correlations have been developed in the extended range. To generate these correlations, the leading surface average and the trailing surface average of the Nu/Nu_s ratios in each pass was plotted as a function of the buoyancy parameter as shown in Fig. 13. In this figure, comparisons are made with

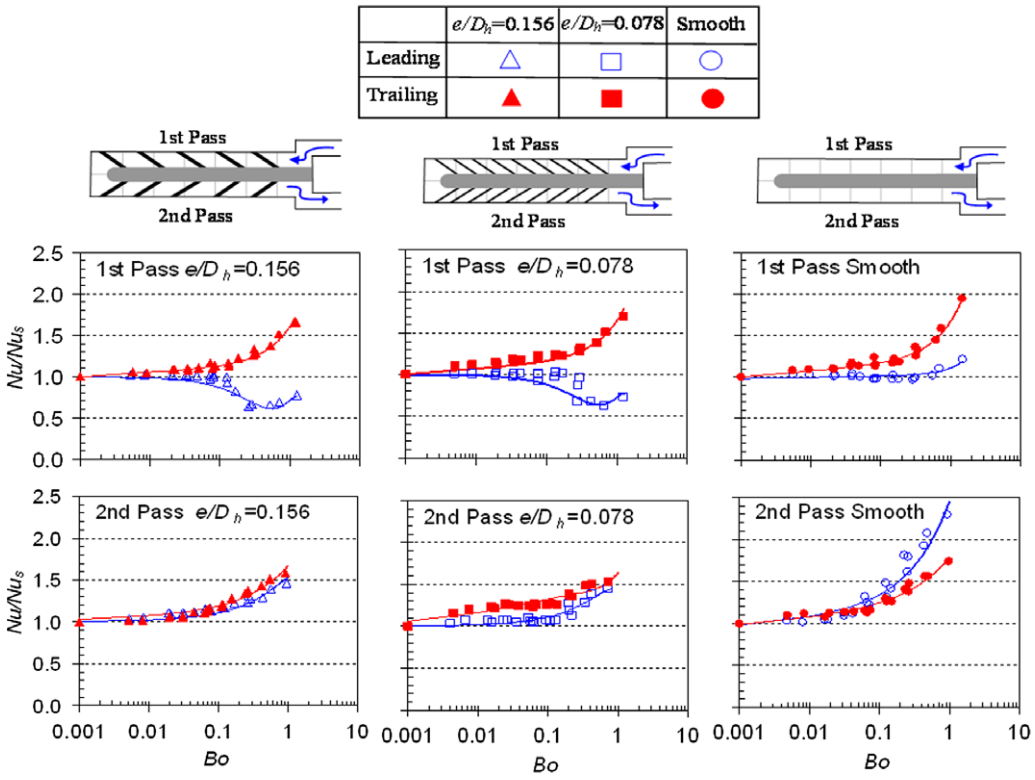

Fig. 13. Comparison of first pass and second pass average leading and trailing surface *Nu* ratios (*Nu/Nus*) as a function of buoyancy parameter (*Bo*) for the current study (*P/e* = 10, *e/Dh* = 0.156), Huh et al. [8] (*P/e* = 10, *e/Dh* = 0.078), and Liu et al. [17] (smooth).

two previous studies (Huh et al. [8] and Liu et al. [17]). The stationary Nusslet number (Nu_s) was chosen as the denominator so that the effects of rotation can be seen.

The importance of this figure is clear when considering the averaged Nu/Nu_s ratios on the leading surface in the first pass. The two ribbed cases show a very different trend when compared to the smooth case. The averaged Nu/Nu_s ratios on the leading surface for the smooth case are not affected by the buoyancy parameter until the maximum buoyancy parameter value of almost 2.0. This is due to the strong entrance effect. The two ribbed cases show nearly Nu/Nu_s ratios trends on both the leading and trailing surfaces in the first pass. This implies that the effect of rotation for both blockage ratios (e/D_h) compared in this study is the same; even though the blockage ratio in this study was twice that of Huh et al. [8].This lack of difference may be due to the large distance between the leading and trailing surfaces in the 1:4 aspect ratio channel.

Another point to make is that the presence of the ribs on the leading surface in the first pass diminishes the effect of the entrance. This statement is drawn from the observation that the averaged Nu/Nu_s ratios drop to a value of nearly 0.5 for the ribbed cases, whereas the averaged Nu/Nu_s ratios for the smooth case stay nearly constant at 1.0 and actually increase at the highest buoyancy parameter value. Contrarily, the averaged Nu/Nu_s ratios on the trailing surface in the first pass do not seem to be altered by the presence of the ribs.

In the second pass, the averaged Nu/Nu_s ratios for the ribbed cases again are similar to each other in that the effect of rotation is reduced when compared to the smooth channel. For both ribbed cases, the averaged Nu/Nu_s ratios on the leading and trailing surfaces are about 1.5 at the maximum buoyancy parameter. However, the smooth case, the leading surface shows a stronger dependence on rotation and a maximum averaged Nu/Nu_s ratio of 2.25 is reached at the highest buoyancy parameter. Also notice that a clear difference in averaged Nu/Nu_s ratios on the leading and trailing surfaces is seen for the smooth channel. For the $e/D_h = 0.078$ case the difference in averaged Nu/Nu_s ratios between the trailing and leading surface decreases. Finally, for the $e/D_h = 0.156$ case, it is seen that the averaged Nu/Nu_s ratios for the leading and trailing surfaces is nearly identical.

Fig. 13 also shows the correlations for each ribbed case and the smooth case. The power law function used to correlate the data is shown in Eq. (9). The corresponding coefficients and exponents for the three different cases are listed in Table 1.

$$Nu/Nu_s = A \cdot Bo^a + B \cdot Bo^b + C \cdot Bo^c + D \quad (9)$$

The discrepancy between experimental and predict values of averaged Nu/Nu_s ratios for the current study was ±12% for the leading surface and ±7% for the trailing surface in the first pass. In the second pass the leading surface had a discrepancy of ±7% and the trailing ±6%. The discrepancy for the other two cases is also shown in Table 1.

4.7. Averaged heat transfer

To further investigate the differences between the two ribbed cases and the smooth channel, the pass averaged stationary Nu_s/Nu_o ratios are plotted as a function of the Reynolds number as shown in Fig. 14. In the first pass and second pass, it is seen that the Nu_s/Nu_o ratios for both blockage ratio cases decrease with an increase in Reynolds number. At a Reynolds number of 10 K, the $e/D_h = 0.156$ case has the highest Nu_s/Nu_o ratio in both the first pass and second pass. It seems then that at the low Reynolds number of 10 K, the secondary flow of the taller rib ($e/D_h = 0.156$) may be stronger compared to the shorter rib ($e/D_h = 0.078$).

In the first pass, for a Reynolds number of 15 K or more, the two blockage ratios have nearly identical Nu_s/Nu_o ratios. This is due to the entrance of the channel. In the second pass, for a Reynolds number of 15 K or more, the Nu_s/Nu_o ratios for the $e/D_h = 0.156$ case are almost the same as the $e/D_h = 0.078$ case. This is due to the effect of the sharp 180° turn.

Fig. 14 also shows how the condition (smooth or ribbed) of the adjacent leading and trailing walls affects the Nu_s/Nu_o ratios on the tip cap. Tip 6, which is in the first pass, shows similar Nu_s/Nu_o ratios for all ribbed cases and smooth case for a Reynolds number of 15 K or less. However, at the larger Reynolds numbers (20–40 K) the Nu_s/Nu_o ratios for the ribbed cases are below the smooth case. However, no difference in Nu_s/Nu_o ratios is seen between the two blockage ratios tested. A similar pattern is seen for tip 7 for a Reynolds number of 20–40 K.

Table 1
Coefficients, exponents and discrepancy values for Nu/Nu_s correlations (T, trailing; L, leading; 1, first pass; 2, second pass).

Discrepancy	L1 ±12%	T1 ±7%	L2 ±7%	T2 ±6%
$e/D_h = 0.156$				
A	−1.73	1.25	−1.50	1.10
B	3.49	0.48	1.51	0.57
C	−2.05	−0.19	0.52	0.00
D	1.00	0.06	1.00	0.00
a	2.65	0.04	2.10	0.01
b	2.04	1.10	2.00	0.69
c	1.10	0.21	0.70	0.00
	±16%	±9%	±8%	±8%
$e/D_h = 0.078$				
A	−1.75	1.30	−1.60	3.30
B	3.48	0.48	1.51	−5.00
C	−2.00	−0.19	0.52	2.34
D	1.00	0.06	1.00	1.00
a	2.69	0.04	2.10	1.15
b	2.09	1.10	1.85	0.90
c	1.14	0.21	0.70	0.51
	±5%	±6%	±15%	±9%
Smooth				
A	1.00	1.23	1.20	1.21
B	0.04	0.44	1.25	0.57
C	0.05	0.00	0.00	0.00
D	0.02	0.00	0.00	0.00
a	0.01	0.03	0.03	0.03
b	2.00	1.20	0.75	0.69
c	1.20	0.00	0.00	0.00

5. Conclusions

In the current study, experimental heat transfer tests were performed in a 1:4 aspect ratio channel. Ribs were placed on the leading and trailing walls of the channel in both the first pass and second pass. Two different blockage ratios were tested. From this research, the following conclusions have been made:

1. The entrance effect dominates over the rotation effect on the trailing surface at the entrance region while the opposite is true for the leading surface.
2. The effect of rotation in the first pass (downstream from the entrance), serves to increase the heat transfer on the trailing surface significantly ($Nu/Nu_s = 2.0$), and decrease the heat transfer on the leading surface significantly to values of $Nu/Nu_s = 0.5$. A critical rotation number exists ($Ro = 0.3$) after which an increase in heat transfer occurs on the leading surface.
3. The effect of rotation in the second pass (downstream of the turn) decreases. Only slight increases in the heat transfer on both surfaces are observed. The difference in Nu/Nu_s ratios between the leading and trailing surfaces is very small.

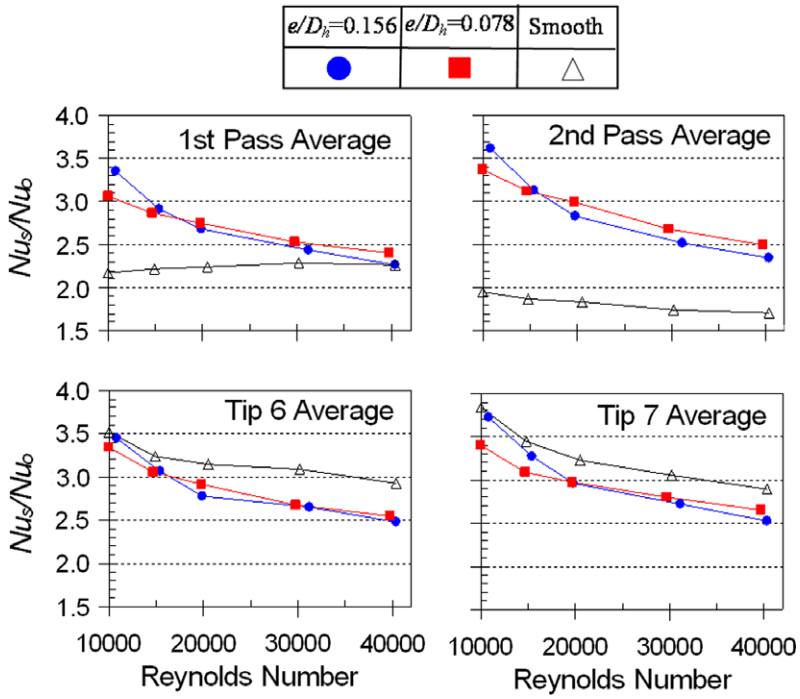

Fig. 14. Comparison of first pass, second pass and tip cap average *Nu* ratios (Nus/Nu_o) as a function of Reynolds number (*Re*) for the current study (*P/e* = 10, *e/Dh* = 0.156), Huh et al. [8] (*P/e* = 10, *e/Dh* = 0.078), and Liu et al. [17] (smooth).

4. In the tip portion, the effect of rotation is to increase heat transfer for both the leading and trailing tip cap surfaces. In the stationary case, the adjacent ribbed walls caused a decrease in heat transfer compared to smooth.
5. The effect of rotation and stationary pass averaged results is very similar for both blockage ratios (e/D_h) compared in this study. This is due to the large distance between the leading and trailing surfaces, the sharp entrance and sharp 180° turn.
6. The rotation number and buoyancy parameter have been extended to values of 0.65 and 1.5 respectively. The correlations developed in this study show that the buoyancy parameter can be used in the higher range to satisfactory levels of accuracy to predict the effects of rotation (Nu/Nu_s).

Acknowledgment

This work has been funded through the Marcus Easterling Endowment Fund.

References

[1] J.C. Han, S. Dutta, S.V. Ekkad, Gas Turbine Heat Transfer and Cooling Technology, Taylor and Francis, New York, 2000.
[2] J.C. Han, Heat transfer and friction characteristics in rectangular channels with rib turbulators, ASME J. Heat Transfer 110 (1988) 321–328.
[3] J.C. Han, J.S. Park, Developing heat transfer in rectangular channels with rib turbulators, Int. J. Heat Mass Transfer 31 (1988) 183–195.
[4] J.S. Park, J.C. Han, Y. Huang, S. Ou, Heat transfer performance comparisons of five different rectangular channels with parallel angled ribs, Int. J. Heat Mass Transfer 35 (11) (1992) 2891–2903.
[5] J.C. Han, L.R. Glicksman, W.M. Rohsenow, An investigation of heat transfer and friction for rib-roughened surfaces, Int. J. Heat Mass Transfer 21 (1978) 1143–1156.
[6] M.E. Taslim, S.D. Spring, Effects of turbulator profile and spacing on heat transfer and friction in a channel, J. Thermophys. Heat Transfer 8 (1994) 555–562.
[7] J.C. Han, Heat transfer and friction in channels with two opposite rib-roughened walls, ASME J. Heat Transfer 106 (1984) 774–781.
[8] M. Huh, Y.H. Liu, J.C. Han, S. Chopra, Effect of Rib Spacing on Heat Transfer in a Two-pass Rectangular Channel (*AR* = 1:4) with a Sharp Entrance at High Rotation Numbers, ASME Paper No. GT2008-50311, 2008.
[9] J. Guidez, Study of the convective heat transfer in a rotating coolant channel, ASME J. Turbomachinery 111 (1989) 43–50.
[10] J.H. Wagner, B.V. Johnson, T.J. Hajek, Heat transfer in rotating passages with smooth walls and radial outward flow, ASME J. Turbomachinery 113 (1991) 42–51.
[11] J.H. Wagner, B.V. Johnson, F.C. Kooper, Heat transfer in rotating passage with smooth walls, ASME J. Turbomachinery 113 (1991) 321–330.
[12] M.E. Taslim, L.A. Bondi, D.M. Kercher, An experimental investigation of heat transfer in an orthogonally rotating channel roughened with 45 deg criss-cross ribs on two opposite walls, ASME J. Turbomachinery 113 (1991) 346–353.
[13] G.S. Azad, J.C. Han, H.K. Moon, B. Glezer, Heat transfer in a two-pass rectangular rotating channel with 45-deg angled rib turbulators, ASME J. Turbomachinery 124 (2002) 251–259.
[14] L.M. Al-Hadhrami, T.S. Griffith, J.C. Han, Heat Transfer in Two-Pass Rotating Rectangular Channels (*AR* = 2) With Parallel and Crossed 45° V-Shaped Rib Turbulators, AIAA Paper No. 2002-0789, 2002.
[15] W.L. Fu, L.M. Wright, J.C. Han, Heat Transfer in Two-Pass Rotating Rectangular Channels (*AR* = 1:2 and *AR* = 1:4) with 45° Angled Rib Turbulators, ASME Paper No. GT 2004-53261, 2004.
[16] L.M. Wright, W.L. Fu, J.C. Han, Influence of entrance geometry on heat transfer in rotating rectangular cooling channels (*AR* = 4:1) with angled ribs, J. Heat Transfer 127 (2005) 378–387.
[17] Y.H. Liu, M. Huh, J.C. Han, S. Chopra, Heat Transfer in a Two-Pass Rectangular Channel (1:4) Under High Rotation Numbers, ASME Paper No. GT2007-27067, 2007.
[18] S.J. Kline, F.A. McClintock, Describing uncertainty in single-simple experiments, Mech. Eng. 75 (1953) 3–8.
[19] K.M. Kim, Y.Y. Kim, D.H. Lee, D.H. Rhee, H.H. Cho, Influence of duct aspect ratio on heat/mass transfer in coolant passages with rotation, Int. J. Heat Mass Transfer 28 (2006) 353–357.
[20] J.C. Han, P.R. Chandra, S.C. Lau, Local heat/mass transfer distributions around sharp 180 deg. turns in two-pass smooth and rib-roughened channels, ASME J. Heat Transfer 110 (1988) 91–98.
[21] J.C. Han, P. Zhang, Effect of rib-angle orientation on local mass transfer distribution in a three-pass rib roughened channel, ASME J. Turbomachinery 113 (1991) 123–130.
[22] S.V. Ekkad, J.C. Han, Detailed heat transfer distribution in two-pass square channels with rib turbulators, Int. J. Heat Mass Transfer 40 (11) (1997) 2525–2537.
[23] C.W. Park, S.C. Lau, Effect of channel orientation of local heat (mass) distributions in a rotating two-pass square channel with smooth walls, ASME J. Heat Transfer 120 (1998) 624–632.
[24] C.W. Park, C. Yoon, S.C. Lau, Heat (mass) transfer in a diagonally oriented rotating two-pass channel with rib-roughened walls, ASME J. Heat Transfer 122 (2000) 208–211.
[25] T.M. Liou, Y.Y. Tzeng, C.C. Chen, Fluid flow in a 180 deg sharp turning duct with different divider thicknesses, ASME J. Turbomachinery 121 (1999) 569–575.

[26] T.M. Liou, C.C. Chen, LDV study of developing flows through a smooth duct with a 180 deg straight–corner turn, ASME J. Turbomachinery 121 (1999) 167–174.
[27] T.M. Liou, C.C. Chen, M.Y. Chen, Rotating effect on fluid flow in two smooth ducts connected by a 180-degree bend, ASME J. Fluids Eng. 125 (2003) 138–148.
[28] T.M. Liou, C.C. Chen, Heat transfer in a rotating two-pass smooth passage with a 180-deg rectangular turn, Int. J. Heat Mass Transfer 42 (2) (1999) 231–247.
[29] G. Su, H.C. Chen, J.C. Han, D. Heidmann, Computation of Flow and Heat Transfer in Two-Pass Rotating Rectangular Channels ($AR = 1{:}1$, $AR = 1{:}2$, $AR = 1{:}4$) with 45-Deg Angled Ribs by a Reynolds Stress Turbulence Model, ASME Paper No. GT2004-53662, 2004.